Tuning curvature and phase behavior of monoolein bilayers by epigallocatechin-3-gallate: Structural insight and cytotoxicity

Tuning Curvature and Phase Behavior of Monoolein Bilayers by Epigallocatechin-3-gallate: Structural Insight and Cytotoxicity

Cristina Minnelli[1#], Paolo Moretti[1#], Emiliano Laudadio[2], Yuri Gerelli[1], Andrea Pigozzo[3], Tatiana Armeni[4], Roberta Galeazzi[1], Paolo Mariani[1], Giovanna Mobbili[1*]

1 Department DISVA, Università Politecnica delle Marche, via Brecce Bianche, 60131 Ancona, Italy
2 Department SIMAU, Università Politecnica delle Marche, via Brecce Bianche, 60131 Ancona, Italy
3 Alfatest Srl, Cinisello Balsamo (MI), Italy
4 Department DISCO, Università Politecnica delle Marche, via Brecce Bianche, 60131 Ancona, Italy

* Correspondence; g.mobbili@staff.univpm.it; +390712204707
[#] Contribute equally

Short statistical summary

Number of words: 5995

Number of Figures: 5

Number of Tables: 3

Tuning Curvature and Phase Behavior of Monoolein Bilayers by Epigallocatechin-3-gallate: Structural Insight and Cytotoxicity

Cristina Minnelli[1#], Paolo Moretti[1#], Emiliano Laudadio[2], Yuri Gerelli[1], Andrea Pigozzo[3], Tatiana Armeni[4], Roberta Galeazzi[1], Paolo Mariani[1], Giovanna Mobbili[1*]

2 Department DISVA, Università Politecnica delle Marche, via Brecce Bianche, 60131 Ancona, Italy
2 Department SIMAU, Università Politecnica delle Marche, via Brecce Bianche, 60131 Ancona, Italy
5 Alfatest Srl, Cinisello Balsamo (MI), Italy
6 Department DISCO, Università Politecnica delle Marche, via Brecce Bianche, 60131 Ancona, Italy

* Correspondence; g.mobbili@staff.univpm.it; +390712204707
[#] Contribute equally

Abstract

The use of glyceryl monooleate (GMO)-based nanoparticles has not yet been explored in overcoming the low bioavailability of Epigallocatechin-3-gallate (EGCG), a green tea polyphenol with a known anticancer activity. Since the inclusion of a guest molecule can affect the curvature and the supramolecular structure of fully hydrated GMO-based phase, the phase behavior of bulk and dispersed liquid crystalline systems containing EGCG were explored by Small Angle Neutron Scattering and X-Ray Diffraction experiments. Molecular Dynamic Simulations showed how the interaction of EGCG with polar heads of GMO strongly affects the curvature and packing of GMO phase. The EGCG encapsulation efficiency was determined in the nanodispersions and their size studied by Dynamic Light Scattering and Atomic Force Microscopy. A nanodispersed formulation has been optimized with a cytotoxic effect more than additive of GMO and EGCG.
.

Keywords: monoolein; Epigallocatechin-3-gallate; Small Angle Neutron Scattering, X-Ray Diffraction, Dynamic Light Scattering, MD simulations

Introduction

Glyceryl monooleate (1-(*cis*-9-octadecenoyl)-rac-glycerol, GMO) is an amphiphilic lipid featuring a glycerol backbone and a nonpolar hydrocarbon chain attached to the polar head by an ester bond. This structure allows GMO to self-assemble into a variety of liquid crystalline structures under different conditions of temperature and solvent composition. The resulting thermotropic and lyotropic phases can range from simple topologies as spherical micelles and planar bilayers to more complex like hexagonal and bicontinuous cubic phases. These last are three-dimensional periodic lipidic bilayer that can be divided into three types on the base of the crystallographic behavior: the primitive lattice (Q229), the double-diamond lattice (Q224), and the gyroid lattice (Q230). The presence of a relatively small and non-ionic headgroup and the kink in the hydrophobic tail of GMO promotes, in excess water, the formation of a Q224 phase at wide temperature range. This non-lamellar phase consists of two non-intersecting continuous water channels meeting in 4-way junctions at the tetrahedral angle and separated by a lipid layer. The presence of a lipid chain region and an aqueous domain confers to GMO the ability to load both hydrophobic and hydrophilic molecules as well amphiphilic compounds at the water-lipid interface [1].

This feature, combined with the resemblance to biomembrane structures and with the ability to extend the release of bioactive substances, makes monoolein-based cubic liquid crystals potential delivery systems to be employed in the improvement of the stability and cellular uptake of molecules presenting a poor bioavailability. The powerful antioxidant epigallocathechin-3-gallate (EGCG) is the major constituent of catechins present in green tea. It exhibits several health-promoting effects, such as antioxidant, anti-inflammatory, anti-obesity, and antitumor activities [2, 3]. These biological benefits cannot be simply correlated to its action as radical scavenger and metal chelator since the EGCG structure allows it to interact with a wide range of biological targets [4]. This ability is particularly evident in the EGCG anticancer activity by which it downregulates the expression and activity of several cancer-related receptors, therefore inhibiting cell proliferation [5]. Although numerous preclinical studies have demonstrated the potential therapeutic benefits of EGCG, pharmacokinetic studies performed on humans reported that EGCG has a low oral bioavailability [6] that can be enhanced by the employment of an appropriate vector. Several types of nanovehicles were adopted at this purpose including lipid-, carbohydrate- and protein-based nanoparticles [7-9]. However, its encapsulation inside monoolein nanoparticles has not yet been explored.

In this work we encapsulated EGCG in GMO LLC (lyotropic liquid crystals) and chose as stabilizer the amphiphilic poly(ethylene oxide)–poly(propylene oxide) (PEO–PPO)-based copolymer Poloxamer-407. Because the addition of guest molecules can influence the phase behavior of the binary GMO/water system, a structural study was carried out by Small Angle Neutron Scattering (SANS) and X-Ray Diffraction (XRD) experiments to investigate the effect of Poloxamer-407 and EGCG on the monoglyceride mesophase structure. Molecular dynamics (MD) simulations have been used to better clarify how the EGCG can promote monoolein phase changes by disturbing the delicate balance between the headgroup and the tail volume in the Q224 phase. With the aim to explore the delivery efficiency, the cytotoxicity of EGCG-loaded GMO nanoparticles was evaluated *in vitro* in human lung adenocarcinoma cell line (A549) by means of cellular metabolic evaluation (MTT assay).

Experimental

Materials

Glyceryl monooleate (monoolein, GMO), Sephadex G-50, Poloxamer-407 ($PEO_{98}POP_{67}PEO_{98}$), Triton-X100, 3-(4,5-dimethylthiazol-2-yl)-2,5-diphenyl-tetrazolium bromide (MTT) and Folin-Ciocalteu reagent were obtained from Sigma Aldrich (St. Louis, MO, USA. Epigallocatechin-3-Gallate was purchased from Cayman Chemical Company (Ann Arbor, MI, USA). The human lung adenocarcinoma epithelial cell line (A549) was obtained from American Type Culture Collection (ATCC), Italy.

Preparation of EGCG loaded bulk lipid phases and their dispersed forms

The EGCG-loaded bulk liquid crystalline phases (EB) and the corresponding nanodispersions (ES) were prepared by thin film hydration method [10] using GMO (4% w/w) and a GMO/Poloxamer-407 binary system (4:1, w/w), respectively. The dried films were hydrated with PBS solutions containing increasing amount of EGCG and left to

equilibrate for 48 h at 25°C. The viscous bulk phases were diluted with PBS and sonicated by a probe sonicator (QSonica Q125) (10 min; 1 sec on; 1 sec off; 50%) at 0 °C to obtain nanodispersions. The final concentrations of GMO and Poloxamer-407 were 2.5% and 0.63% w/w, respectively. The final amount of EGCG in both bulk and dispersed phase was 5, 10, 18 and 25% w/w with respect to the monoolein.
The EB were directly used for XRD and SANS experiments, while ES were employed for Dynamic Light Scattering (DLS) and Atomic Force Microscopy (AFM) characterization, SANS experiments, encapsulation efficiency determination, and cellular assays.

EGCG encapsulation
The EGCG-loaded nanodispersions were purified from the free EGCG by size exclusion chromatography [3]. After separation of EGCG-loaded nanodispersions from free EGCG, the encapsulation efficiency was obtained by lysing purified and unpurified nanoparticles with 1% Triton X-100; the EGCG concentration was quantified by the Folin-Ciocalteu assay [11]. The absorbance was measured at 765 nm on a BioTek Synergy HT MicroPlate Reader Spectrophotometer. The Encapsulation Efficiency (EE) and Loading Capacity (LC) were determined by using the following formulas:

$EE\ (\%) = 100 \times [(C_{int})/ C_{total}]$
$LC\ (\%) = 100 \times [(C_{int})/ C_{lipid}]$

where the C_{total} is the total concentration of EGCG, C_{int} refers to the concentration of the encapsulated molecule, and C_{lipid} is the total lipid concentration. All the experiments were repeated at least three times and measurements were run in triplicate.

X-Ray Diffraction
XRD experiments were performed using a 3.5 kW Philips PW 1830 X-ray generator (Amsterdam, Netherlands) provided with a bent quartz crystal monochromator (λ=1.54 Å) and a Guinier-type focusing camera (homemade design and construction, Ancona, Italy). Diffraction patterns were recorded on GNR Analytical Instruments Imaging Plate system (Novara, Italy). Samples, held in a tight vacuum cylindrical cell provided with thin mylar windows, were analyzed at 25°C.
In each experiment, Bragg peaks were detected. The peaks observed in the low-angle region were indexed considering the different symmetries commonly observed in the monoolein phase diagram (cubic, hexagonal, or lamellar [1, 12] and the unit cell dimension of the phase, *a*, calculated from the averaged spacing of the observed peaks.

Small Angle Neutron Scattering
SANS experiments were performed on the diffractometer D22 (Institut Laue-Langevin, Grenoble) at 20 °C, using neutrons with a wavelength of 6 Å and three sample-to-detector distances (1.5 m, 5.6 m and 17.6 m), corresponding to a Q-range from 0.003 to 0.6 $Å^{-1}$. Sample solutions were transferred into 1 mm thick flat quartz cells prior to the measurement. To maximize the scattering intensity from fully hydrogenated samples, D_2O was used instead of H_2O. 2D detector images were reduced and converted into I(Q) curves (in absolute units)

using GRASP (a Matlab™ script application produced by ILL). Merging and background subtraction was performed using the SANS reduction macros provided by NIST Center for IGOR [13].

Atomic Force Microscopy

AFM measurements were carried out on an AIST-NT's Scanning Probe Microscopy, (Horiba Scientific). Images were generated in non-contact mode with a pyramidal silicon tip, with radius of 8 nm. For improving the quality of the measurements, samples were diluted from the original concentration by 1:1000. 5 microliters of the diluted solution were deposited on a freshly cleaved mica surface and then dried by nitrogen blow down. All images were acquired with a resolution of 512x512 pixels with a scan rate of 1 Hz and were analysed with the AIST-NT software (Horiba) and ImageJ software.

Computational methods

All energy calculations were carried out using LOPLS-AA all-atom force field for long hydrocarbon chains; this force field is an OPLS-AA based force field, with an implemented parametrization to treat accurately alcohols, esters, and glyceryl monooleate (GMO) lipids. The torsion profiles concerning alcohol and ester groups relevant for GMO parametrization have been refitted to relative quantum chemistry energies at MP2/aug-ccpVTZ level of theory estimated on MP2/cc-pVDZ optimized geometries [14]. Atomistic Molecular dynamics (MD) simulations were carried out using an integration step size of 2 fs, and the electrostatic interactions beyond a real-space cutoff of 1.5 nm were calculated using the Particle Mesh Ewald (PME) method [15]. A long-range correction for both energy and pressure was applied, while van der Waals interactions were switched to zero between 1.1 and 1.3 nm [16]. The temperature was kept constant at 298 K using the velocity rescale thermostat with τ=0.1 ps. The pressure was isotropically coupled using Parrinello−Rahman barostat [17] with setting reference pressure to 1 bar. All covalent bonds to hydrogen atoms were kept at constant lengths applying LINCS algorithm. Water was described by the TIP3P model [18].

Four systems for self-assembly simulations were then prepared. For each system, 544 randomly rotated GMO molecules were placed on cubic grids of 6 nm^3 dimension using Packmol software [19]. 3592 TIP3 water molecules (resulting in water w/w percentage ratio of 25 % respect to GMO molecules) were randomly added in each system to properly mix lipid compounds with water molecules. EGCG molecules were explicitly added in three of the four systems, to reach EB-5%, EB-10%, and EB-18%. Each system underwent 200 ns of MD simulation at 298 K, and the *volume-per-lipid* variations of the GMO systems were evaluated on the time interval from 190 to 200 ns. Periodic boundary conditions (PBC) were considered for all boxes' axes [20]. All MD simulations were performed using GROMACS 5.0.5 suite [21], while the trajectories analysis was performed using CHIMERA [22] and VMD [23] programs. Computation of each MD trajectory was carried out on MARCONI-100 (CINECA-HPC ISCRA project n. HP10CMPMGP).

Dynamic Light Scattering and ζ-potential

The intensity-based diameter (Z-average), the polydispersity index (PDI) and ζ-potential values of liposomes were measured by Dynamic Light Scattering (DLS) and Electrophoretic Light Scattering using a Malvern Zetasizer Nano ZS (Malvern Instruments GmbH, Marie-Curie-Straße 4/1, 71083 Herrenberg, Germany). Measurements were performed at 25 °C with a fixed angle of 173°. For all samples investigated, the data represent the average of at least three different autocorrelations carried out for each sample.

Biological Experiments

Cytotoxicity studies of GMO-based nanoparticles was performed after separation of the nanodispersions from the untrapped EGCG on human lung adenocarcinoma cell line (A549). Cells were seeded in 24-well plates at $15x10^3$/well to reach 50-60% of confluence at 24 h; then, A549 were treated with empty and EGCG loaded GMO-nanoparticles for 72 h. The results were compared with the correspondent concentrations of bare EGCG. The number of metabolically active cells was assessed by MTT assay as previously described and the absorbance at 570 nm was read [3]. The relative cell viability (%) was calculated as (A570 of treated samples/A570 of untreated samples) x 100. Determinations were carried out in triplicate in each experiment and mean ± SD from five independent experiments was calculated.

Statistical Analyses

Data are presented as mean ± S.D. Statistical comparison of differences among groups of data was carried out using Student's t-test. $P \leq 0.05$ were considered statistically significant, $P \leq 0.001$ were considered highly significant.

Results

1. Preparation and EGCG entrapment studies of bulk cubic phases and cubic phase nanodispersions

The composition of EGCG-loaded bulk (EB) and dispersed cubic phases (ES), prepared with increasing EGCG concentrations (%w/w of EGCG on GMO, 5, 10, 18, 25%), is shown in **Table 1.** After ultrasonic dispersion process, all the GMO/Polox dispersed formulations (ES) obtained from viscous liquid crystalline phases (EB) appeared opalescent except for ES-25% in which a few of yellow precipitates was observed. The encapsulation efficiency (EE) in EB significatively decreased as the concentration of EGCG increases from formulation containing 5% of drug (EB-5%) to those containing higher EGCG concentrations (EB-10%; EB-18%; EB-25%) (**Table 1**). As for the EB, the EE of the dispersed phases (ES) decreased from ES-5% to one's ES-25%; however, the formulation containing 18% of EGCG departs from this trend showing 51% of EGCG encapsulation. Regarding the Loading Capacity (LC) a progressive increase in the amount of total entrapped EGCG with respect the total lipid weight, in both EB and ES, was obtained. In particular, the LC doubled until a plateau is achieved at 25% of EGCG concentration.

Table 1. Composition and properties of investigated bulk cubic phases (EB) and cubic phase nanodispersions (ES)

	Content (% w/w)	(% ± SD)

Formulation (% w/w, EGCG/GMO)	GMO	H_2O	Poloxamer-407	EGCG	Encapsulation Efficiency (EE)	Loading Capacity (LC)
Blank-EB	4	96.0	-	-	-	-
EB-5%	4	95.8	-	0.2	48 ± 4	2.1 ± 0.3
EB-10%	4	95.6	-	0.4	34 ± 4	3.4 ± 0.5
EB-18%	4	95.3	-	0.7	33 ± 3	5.8 ± 0.2
EB-25%	4	95.0	-	1.0	29 ± 7	7.2 ± 1.7
Blank-ES	2.5	96.87	0.63	-	-	-
ES-5%	2.5	96.74	0.63	0.13	45 ± 1	2.3 ± 0.4
ES-10%	2.5	96.62	0.63	0.25	40 ± 1	4.1 ± 0.2
ES-18%	2.5	96.43	0.63	0.44	51 ± 4	9.0 ± 0.6
ES-25%	2.5	96.24	0.63	0.63	35 ± 6	8.7 ± 1.4

2. Dimensional Distribution by DLS and AFM

All the dispersions, except for ES-25%, present a high colloidal stability with a monomodal dimensional distribution (PDI<0.3); the intensity mean diameter, expressed as Z-average, ranges from 220 to 300 nm also after 1 month of preparation (**Table 2**). It appears evident that the high EGCG concentration in ES-25% induces a significative increase of nanoparticle mean diameter (t=0, 344 ± 8 nm) ($P<0.05$) and polydispersity index (0.7 ± 0.1 nm) with respect to empty GMO (t=0, 264 ± 4 nm) ($P<0.05$). The Z-average size already increased after 24 h (about 650 nm), and after 1 month of preparation the system was completely precipitated. Due to its high colloidal instability the sample was not used for further investigations on the nanodispersed formulation. The electrostatic potential of the nanoparticles at the shear face was slightly negative for all the formulations but the increasing EGCG concentration induced a significative decrease in ζ-potential absolute value ($P<0.05$) versus neutral values (ζ-potential>-30 mV). Despite these, the presence of Poloxamer-407 prevented the aggregation phenomena as indicated by the dimensional analyses.

Table 2. Colloidal stability of nanostructured lipid particles at different times and conditions.

Formulation	Time	Mean diameter ± SD (nm)	PDI ± SD	ζ-potential ± SD (mV)
GMO	0 h	264 ± 4	0.13 ± 0.03	- 33.5 ± 0.9
	24 h	254 ± 7	0.27 ± 0.02	
	1 month	290 ± 10	0.19 ± 0.03	
ES-5%	0 h	257 ± 3	0.21 ± 0.01	- 27.6 ± 1.5
	24 h	288 ± 4	0.22 ± 0.01	
	1 month	245 ± 5	0.13 ± 0.08	
ES-10%	0 h	284 ± 2	0.23 ± 0.06	- 24.3 ± 0.2
	24 h	310 ± 5	0.23 ± 0.05	
	1 month	270 ± 6	0.11 ± 0.01	
ES-18%	0 h	229 ± 3	0.24 ± 0.01	-19.2 ± 0.8
	24 h	226 ± 3	0.23 ± 0.01	
	1 month	277 ± 4	0.15 ± 0.02	

ES-25%	0 h	344 ± 8	0.7 ± 0.1	-21.1 ± 0.8
	24 h	650 ± 75	0.68 ± 0.18	
	1 month	-	-	

AFM measurements were performed to obtain the size distribution at the level of the individual particles. In **Figure 1A-C** are reported the non-contact mode images of ES-10% and ES-18% samples, clearly showing the presence of individual particles.

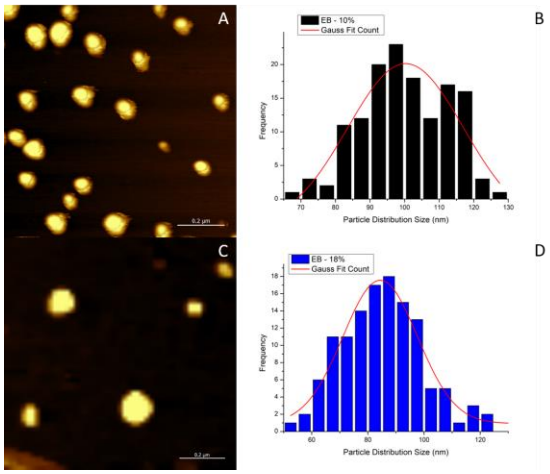

Figure 1. A-C) AFM images aquired in non-contact mode for ES-10% (scalebar 0.2 μm) and ES-18% (scalebar 0.2 μm). **B-D)** Size distribution obtained from the statistical analysis of AFM images for ES-10% **(B)** and ES-18% **(D)**.

Using the ImageJ software (version 1.8.0), a statistical measurement of the average particle size (diameter) was performed on an area of 1 μm^2 and on a large enough number of particles (>150 for each sample). According to a gaussian distribution, the average size resulted 100 nm (with PDI 0.17) for the ES-10% sample and 84 nm (with PDI 0.16) for ES-18% (**Figure 1B-D)**. AFM measurements are in line with DLS measurements indicating that samples prepared at higher EGCG content are characterised by smaller size. On the other hand, the absolute size values obtained by AFM differ significantly from those of the same particles in solution, due to the dilution and drying processes necessary to perform AFM experiments.

3. Effect of EGCG Encapsulation on Bulk Phase and Nanodispersions Structure

X-Ray Diffraction experiments were performed in the high-Q region on EB samples as a function of EGCG concentration, in both the absence and the presence of Poloxamer-407.

SANS data were collected to investigate the morphology (low-Q region) and the internal structure (high-Q region) of EB samples (without Poloxamer-407) and of ES samples.
The inspection of the I(Q) curves obtained from the SANS experiments, reveals a constant intensity increase and no features in the low-Q regime for both type of samples, bulk and nanodispersed structures (**Figure 2A**). The absence of a Guinier region in the Q-range experimentally accessible (data not shown) indicates that the average size of these structures is larger than 200 nm, confirming thus the results obtained by DLS for nanodispersed samples.

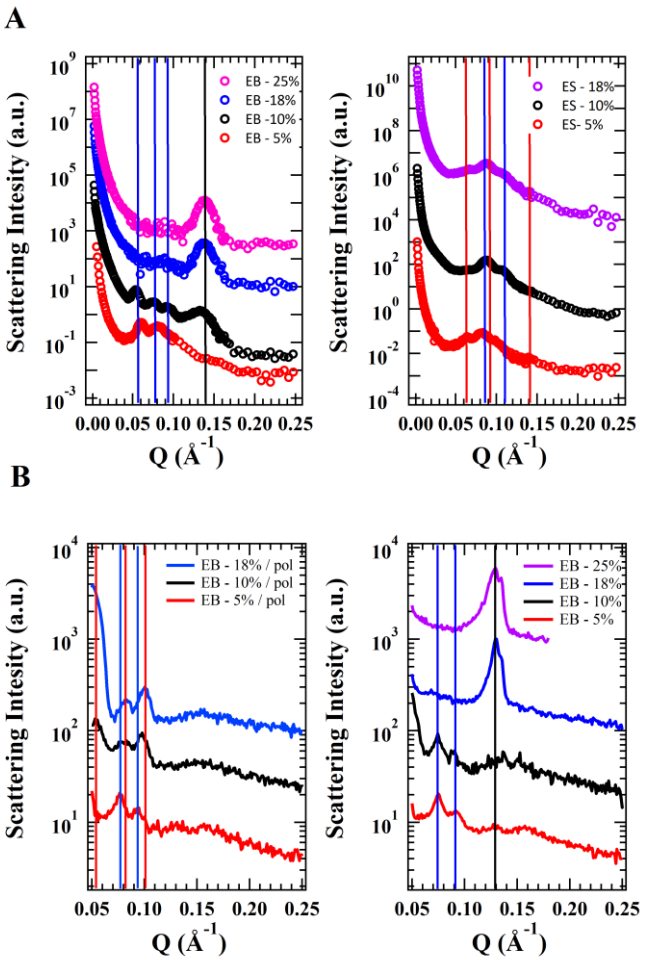

Figure 2. **SANS and XRD experiments. (A)** SANS profiles obtained by bulk samples (left panel) and for nanodispersions in presence of poloxamer (right panel). **(B)** XRD profiles obtained for bulk samples, prepared in the presence (left panel) and in the absence (right panel) of poloxamer. The vertical lines indicate the position

of Bragg peaks for the Q224 cubic phase (blue), and for the lamellar phase (black) and for the Q229 cubic phase(red).

Commentato [MC1]: Mi sembra che solo ES-18% IN ALTO A DESTRA DOVREBBE ESSERE blu

For bulk samples prepared in the absence of Poloxamer-407, XRD profiles show a transition from a cubic Q224 phase, at low EGCG content, to a lamellar phase, occurring in the presence of a large amount of the drug (**Figure 2B,** left panel). These data are confirmed by SANS measurements as shown in **Figure 2A** (left panel). The amplitude of the peaks corresponding to the different phases differs among the two techniques mostly because of the different sensitivity of the probes for selected portions of the samples. However, from the inspection of SANS data it is possible to highlight the formation of the lamellar phase at 10% EGCG content. In this condition, the Q224 and lamellar phases coexist. From the peak positions, the unit cells for the cubic and the lamellar phases have been determined: interestingly, they appear rather constant, even in the biphasic region, and centred to 112 Å for the cubic phase and to 48 Å for the lamellar one. This phase behaviour changes in presence of Poloxamer-407, as the polymer appears to stabilize the cubic structure. Indeed, the EB-5%/polox sample resulted organised in a Q224 cubic phase, while this phase transitioned in a Q229 in EB 10%/polox and EB-18%/polox samples (**Figure 2B**, right panel). The presence of Poloxamer-407 therefore hinders the formation of the lamellar phase observed for pure EB samples. Also in these cases, the dimension of the unit cells is rather independent on EGCG concentration and is centred at 109 Å in Q224 and at 150 Å in Q229. The latter corresponds to a mean curvature of the lipid-water interface of 0.0091 $Å^{-1}$. Analysis of diffraction measurements on nanodispersed samples were carried out only for SANS profiles, due to the very weak scattering presented by these samples during XRD experiments. As observed in the case of bulk samples (EB/Polox), nanodispersed samples prepared with Poloxamer-407 are organised in cubic phases. In particular, a Q224 and a Q229 phase coexist at all the considered EGCG content (**Figure 2A**, right panel). They are characterized by unit cell parameters of 140 Å for the Q229 cubic phase and 111-101 Å for the Q224 phase. The latter is dependent on the EGCG content as indicated by the shift in peak position visible in **Figure 2A** (right panel) going from ES-5% (111 Å) to ES-10% (101 Å). The unit cell remains of 101 Å for higher drug contents. As in the case of bulk samples, the transition to a lamellar phase was not observed, confirming the ability of the Poloxamer-407 to stabilise cubic structures.

4. EGCG and GMO interactions: *in silico* simulations

EGCG influence on monoolein assembly was evaluated using a MD simulation approach. The composition of the unit cell requires setting the proper periodic boundary conditions (PBC) to mimic an infinite system considering a finite number of molecules inside the box [24].

Each of the four systems (GMO, EB-5%, EB-10%, and EB-18%) underwent 200 ns MD simulations and different GMO orientation were found. In details, monoolein molecules went to a self-assembled cubic phase when EGCG molecules were not present (**Figure 3A**). In EB-5% system, monoolein molecules appeared to maintain the cubic phase, while EGCG molecules were placed in the water pore, close to the GMO polar headgroups (**Figure 3B**).

In EB-10% system, EGCG more strongly interacted with monoolein polar headgroups, thus determining a variation in the three-dimensional lipids' disposition (**Figure 3C**) looking as lamellar-like phase. The strong interaction between EGCG and GMO resulted the main force to drive the phase transition. This result was confirmed by the fourth system in which more EGCG was added (EB-18%). In this case, due to a higher amount of catechin molecules that interacts with GMO structures, an ordered lamellar phase was observed (**Figure 3D**), confirming the existence of a dose-dependent effect of EGCG on the lipid phase transition.

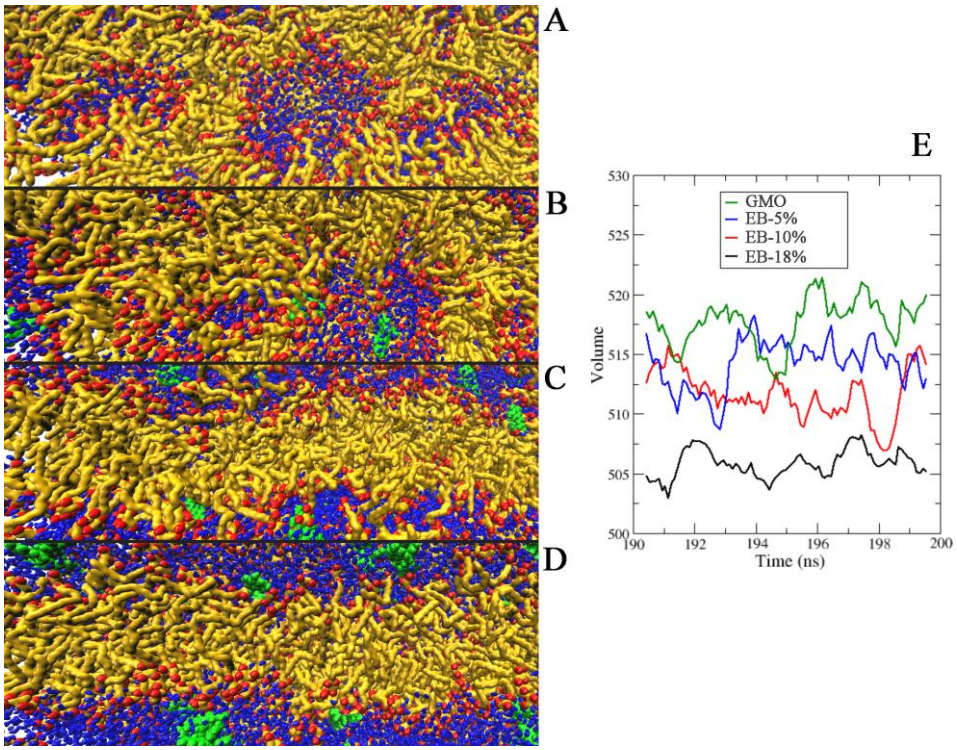

Figure 3. Snapshots of the GMO systems without **(A),** EB-5% **(B)**, EB-10% **(C),** and EB-18% **(D).** EGCG is reported in green VdW spheres; GMO in yellow Quick Surface; polar lipid headgroups in red VdW spheres and water in blue Quick Surface. **(E)** GMO volume per lipid in different studied systems.

The different monoolein displacements were correlated to the different *volume per lipid* values extrapolated from MD simulations. A gradual reduction of GMO *volume per lipid* was found in relation to a gradual decrease of curvature induced by EGCG amount (**Figure 3E**), showing monoolein volume per lipid values of 517.3 ± 5 Å^3, 514.2 ±5 Å^3, 511.1 ± 4.5 Å^3, and 507.5 ± 2.5 Å^3 for GMO, EB-5 %, EB-10 %, and EB-18 % respectively.

With the aim to validate the reproducibility of the obtained results, a direct comparison between *area per lipid* values for the EB-18% system and those obtained experimentally reported in literature for GMO lamellar phase was done [25]. The calculated *area per lipid* value was extrapolated dividing the previously described volume per lipid (507.5 Å^3) by the

average length of the oleic acid (namely 14.5 Å). The computed monoolein *area per lipid* in EB-18% system resulted 35 Å^2, in line with experimental evidence for the L_α GMO phases at room temperature [26]. This comparison between computational and experimental data confirmed the strong effect of EGCG on the influencing the GMO disposition.

5. Cytotoxicity effect of GMO-based cubosomes

The potential anti-cancer application of GMO-based LCC loaded with EGCG (ES) has been evaluated in human lung carcinoma A549 cell lines. As shown in the **Figure 4A-B**, ES-Blank induced a dose-dependent decrease in cell viability with an IC50 (50% growth inhibition) of 106 μg/ml (**Table 3**).

Table 3. Determined IC50 values in A549 cells exposed for 72 h to different treatments. Error ± S.D. (n=5).

Formulation	IC50 [Lipid, μg/mL] ± SD	Correspondent [EGCG, μM]
ES-Blank	106 ± 3	0
ES-5%	98 ± 4	7.8
ES-10%	85 ± 2	11.2
ES-18%	66 ± 4	20.6

The system containing the lowest EGCG concentration (ES-5%) did not show any additional cytotoxic effect with respect to the administration of empty GMO. The others nanoformulations (ES-10% and ES-18%) induced instead a more pronounced decrease of cell viability with an IC50 of 85 and 66 μg/ml, respectively (**Table 3**). Since ES-18% presents a higher encapsulation efficiency respect to ES-10%, at the same lipid concentration administered, the amount of EGCG is different; therefore, to compare nanodispersions cytotoxicity with that of free EGCG we select a 11 μM EGCG concentration which correspond to GMO 36 and 80 μg/mL for the ES-10% and ES-18%, respectively. At this dose, the cytotoxicity of GMO itself did not induce more than to 20% of cell death while the free EGCG decreased cellular viability of 12% with respect to untreated cells (*$p<0.05$). As shown in **Figure 4C**, ES-18% showed the best performance by inducing a decrease in cell viability of 40% with respect empty-GMO treated cells ($P<0.001$).

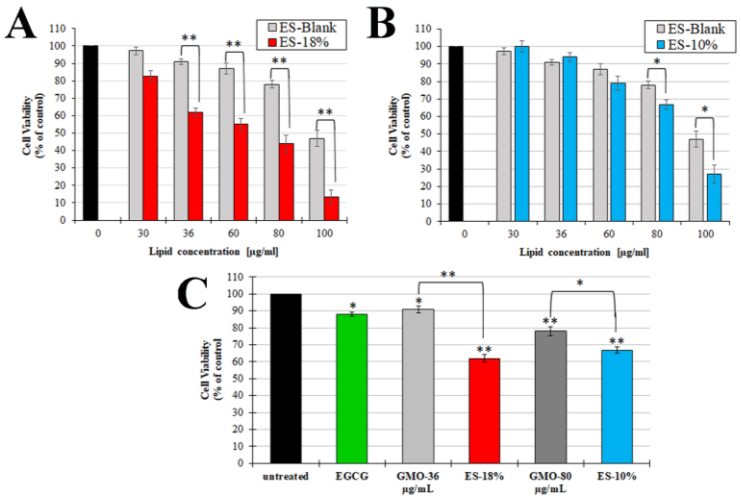

Figure 4. **Cytotoxicity of GMO-based LCC in A549 cell lines. (A-B)** Cells were treated with increasing concentrations of empty and EGCG loaded GMO-based nanoparticles at lipid concentrations range of 0-100 µg/mL for 72 h. **(C)** Cells were treated with 11 µM of EGCG which correspond to 36 and 80 µg/mL GMO concentration for the ES-10% and ES-18%, respectively. Cell viability was measured after 72 h of treatment by MTT assay. Data are expressed as means ± S.D. of five independent experiments, each performed in triplicate.

Discussion

It is known that in excess water GMO forms a Q224cubic phase, but the presence of additives can alter this structure. The structural transitions observed in LLC depends on the spatial stacking of the self-assembling amphiphilic molecules and can be related to the critical packing parameter (CCP). CCP is a measure of the ratio between the portion hydrophilic head and the portion hydrophobic tail of the amphiphilic lipid and is expressed as **CPP = V/al**, where **V** represents the hydrophobic chain volume, **a** the cross-sectional area of the hydrophilic head group, and **l** the tail length. In this work we showed that the encapsulation of increasing EGCG concentrations in GMO prepared in absence of Poloxamer-407 induces a polymorphism in GMO membrane at physiological pH; even small amounts of molecule produce the effect of tuning the internal structure of GMO aggregates (**Figure 5A**); since the unit cell of the Q224 cubic phase for monoolein in excess of water is around 104 Å [28] it is evident that EGCG induces a change in the GMO packing parameter which determines a strong reduction of the mean curvature of the lipid-water interface (from 0.0126 to 0.0091 $Å^{-1}$); it is worth noting that the lamellar phase forming at high EGCG content, has indeed zero curvature

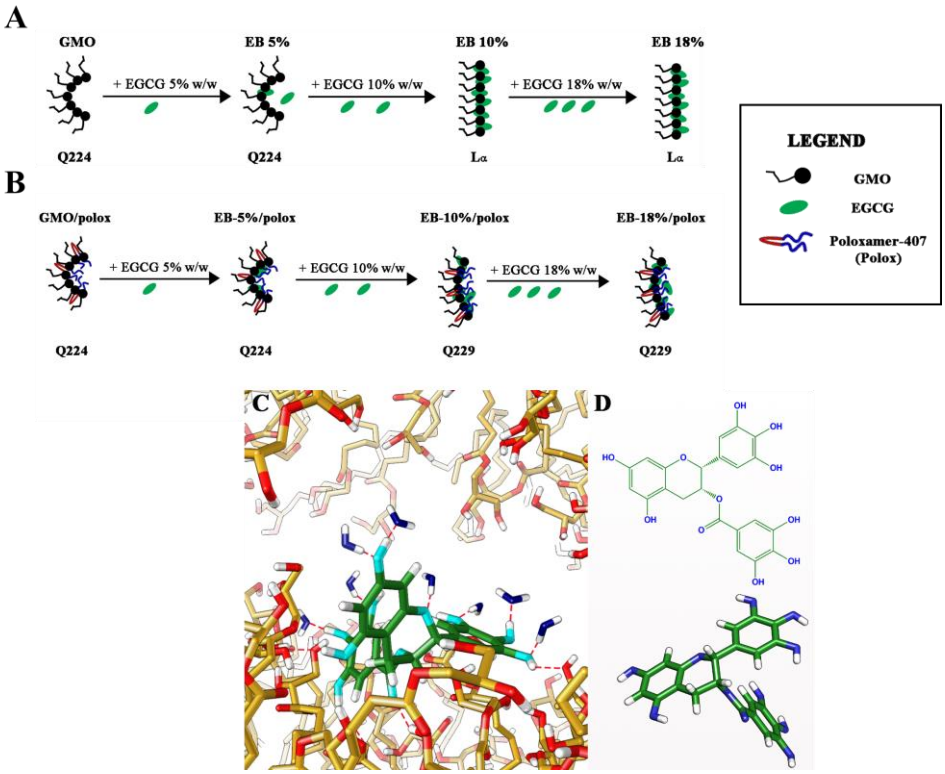

Figure 5. Schematic view of the influence of EGCG on EB phases curvature without **(A)** and with Poloxamer-407 **(B).** EGCG in complex with polar headgroups of GMO and water molecules. C, O, and polar H atoms of GMO are reported in yellow, red, and white, respectively. EGCG is reported in red, water molecules in blue. Note the H bonds reported in red dashed lines **(C).** 2D and 3D structure of EGCG **(D).**

This change can be explained by the interaction of EGCG with polar head of monoolein at the hydrophobic/hydrophilic interface observed in *in silico* simulations (**Figure 5C**); through the formation of a network of hydrogen bonds the polyphenol exhibits a strong ability of increase the effective interface area per molecule, thus reducing the CPP value and inducing the observed phase change. The addition of the Poloxamer-407 is necessary to ensure the colloidal stability of the formulations; the physical instability of ES-25% in terms of precipitations/flocculation is probably due to the formation of a strong hydrogen bond network between EGCG molecules present in solutions and/or on the particles surface. Regarding the influence of Poloxamer-407 on the internal nanostructure of LLC, both SANS and XRD investigations show that the hydrophilic non-ionic surfactant impedes the transition to the lamellar phase also in presence of EGCG, so that GMO maintains a cubic structure (**Figure 5B**). Indeed, in the presence of Poloxamer-407, the samples resulted

organised in a Q224 cubic phase, while this phase transitioned in a Q229 in formulations containing higher EGCG percentage (**Figure 5B**).

The potential application of GMO-based ES cubosomes as EGCG delivery system was studied in A549 by cell growth inhibition evaluation. Both ES-10% and ES-18% were able to potentiate the cytotoxicity of empty GMO and free EGCG (**Figure 4**), but the cytotoxic effect of ES-10% seems to be related to an additive effect, in fact the reduction of cellular viability induced by EGCG nanodispersions (33% fold-decrease with respect to control, $P<0.001$) is equal to the sum of the cytotoxic effect of the two components taken separately (EGCG, 12% and GMO 80 μg/mL, 20%). The ES-18% had instead a higher cytotoxic effect (42% of cell death with respect untreated cells, $P<0.001$) compared to the independent administration of the free EGCG and empty GMO exposed cells (EGCG, 12% and GMO 36 μg/mL, 9%). It is clear that the reason for enhanced toxicity of ES-18% with respect both empty GMO and ES-10% is due to a number of complex factors such as particles size, morphology and effectiveness of the polymeric stabiliser [28, 29]. From the results obtained, one hypothesis is that the different particle size observed for ES-10% and ES-18% (**Table 1**) could promote a different accumulation of EGCG inside cells: from AFM and DLS results, the ES-18% sample showed a mean diameter smaller than ES-10%. By decreasing the size, the surface area of nanoparticles increases facilitating the cellular uptake [30,31] and the internalization of EGCG allowing a greater number of molecules to interact with several biological targets such as Epidermal Growth Factor Receptor (EGFR) [32, 33] and 5'-AMP-activated protein kinase (AMPK) resulting in the growth inhibition of lung cancer cells.

Conclusion

In this work GMO/Poloxamer 407-based nanoformulations have been studied as potential delivery systems of EGCG, a natural molecule with a wide spectrum of biological activities. The influence of EGCG and Poloxamer 407 on the GMO polymorphism has been studied by X-Ray Diffraction and Small Angle Neutron Diffraction. Both the polymer and polyphenol have an impact on the LLC structure due to the location of EGCG near the GMO polar heads. The formulation containing 18% EGCG showed high cytotoxic activity in human lung carcinoma A549 cell lines highlighting an effect more than additive of GMO and EGCG.

Conflicts of Interest: The authors declare no conflict of interest.

References

1. Van'T Hag L, Gras SL, Conn CE, Drummond CJ. Lyotropic liquid crystal engineering moving beyond binary compositional space-ordered nanostructured amphiphile self-assembly materials by design. *Chem Soc Rev*. 2017. doi:10.1039/c6cs00663a
2. Chakrawarti L, Agrawal R, Dang S, Gupta S, Gabrani R. Therapeutic effects of EGCG:

a patent review. *Expert Opin Ther Pat*. 2016. doi:10.1080/13543776.2016.1203419.
3. Minnelli C, Galeazzi R, Laudadio E, et al. Monoalkylated epigallocatechin-3-gallate (C18-EGCG) as novel lipophilic EGCG derivative: Characterization and antioxidant evaluation. *Antioxidants*. 2020. doi:10.3390/antiox9030208
4. Gan RY, Li H Bin, Sui ZQ, Corke H. Absorption, metabolism, anti-cancer effect and molecular targets of epigallocatechin gallate (EGCG): An updated review. *Crit Rev Food Sci Nutr*. 2018. doi:10.1080/10408398.2016.1231168
5. Bimonte S, Cascella M, Barbieri A, Arra C, Cuomo A. Current shreds of evidence on the anticancer role of EGCG in triple negative breast cancer: An update of the current state of knowledge. *Infect Agent Cancer*. 2020. doi:10.1186/s13027-020-0270-5
6. Krupkova O, Ferguson SJ, Wuertz-Kozak K. Stability of (-)-epigallocatechin gallate and its activity in liquid formulations and delivery systems. *J Nutr Biochem*. 2016. doi: 10.1016/j.jnutbio.2016.01.002
7. Granja A, Pinheiro M, Reis S. Epigallocatechin gallate nanodelivery systems for cancer therapy. *Nutrients*. 2016. doi:10.3390/nu8050307
8. Ye JH, Augustin MA. Nano- and micro-particles for delivery of catechins: Physical and biological performance. *Crit Rev Food Sci Nutr*. 2019. doi:10.1080/10408398.2017.1422110
9. Minnelli C, Moretti P, Fulgenzi G, et al. A Poloxamer-407 modified liposome encapsulating epigallocatechin-3-gallate in the presence of magnesium: Characterization and protective effect against oxidative damage. *Int J Pharm*. 2018. doi:10.1016/j.ijpharm.2018.10.004.
10. Esposito E, Eblovi N, Rasi S, et al. Lipid-based supramolecular systems for topical application: A preformulatory study. *AAPS PharmSci*. 2003. doi:10.1208/ps050430
11. Liang J, Cao L, Zhang L, Wan XC. Preparation, characterization, and in vitro antitumor activity of folate conjugated chitosan coated EGCG nanoparticles. *Food Sci Biotechnol*. 2014. doi:10.1007/s10068-014-0078-4
12. Qiu H, Caffrey M. The phase diagram of the monoolein/water system: Metastability and equilibrium aspects. *Biomaterials*. 2000. doi:10.1016/S0142-9612(99)00126-X
13. Kline SR. Reduction and analysis of SANS and USANS data using IGOR Pro. *J Appl Crystallogr*. 2006. doi:10.1107/S0021889806035059
14. Pluhackova K, Morhenn H, Lautner L, et al. Extension of the LOPLS-AA Force Field for Alcohols, Esters, and Monoolein Bilayers and its Validation by Neutron Scattering Experiments. *J Phys Chem B*. 2015. doi:10.1021/acs.jpcb.5b08569
15. Darden T, York D, Pedersen L. Particle mesh Ewald: An N·log(N) method for Ewald sums in large systems. J Chem Phys. 1993. doi:10.1063/1.464397
16. Laudadio E, Galeazzi R, Mobbili G, et al. Depth Distribution of Spin-Labeled Liponitroxides within Lipid Bilayers: A Combined EPR and Molecular Dynamics Approach. *ACS Omega*. 2019. doi:10.1021/acsomega.8b03395
17. Parrinello M, Rahman A. Polymorphic transitions in single crystals: A new molecular dynamics method. *J Appl Phys*. 1981. doi:10.1063/1.328693
18. Sun Y, Kollman PA. Hydrophobic solvation of methane and nonbond parameters of the TIP3P water model. *J Comput Chem*. 1995. doi:10.1002/jcc.540160910
19. Martinez L, Andrade R, Birgin EG, Martínez JM. PACKMOL: A package for building initial configurations for molecular dynamics simulations. *J Comput Chem*. 2009.

doi:10.1002/jcc.21224
20. Minnelli C, Laudadio E, Galeazzi R, et al. Encapsulation of a neutral molecule into a cationic clay material: Structural insight and cytotoxicity of resveratrol/layered double hydroxide/BSA nanocomposites. *Nanomaterials*. 2020. doi:10.3390/nano10010033
21. Weiner SJ, Kollman PA, Singh UC, et al. A New Force Field for Molecular Mechanical Simulation of Nucleic Acids and Proteins. *J Am Chem Soc*. 1984. doi:10.1021/ja00315a051
22. Pettersen EF, Goddard TD, Huang CC, et al. UCSF Chimera - A visualization system for exploratory research and analysis. J Comput Chem. 2004. doi:10.1002/jcc.20084
23. Humphrey W, Dalke A, Schulten K. VMD: Visual molecular dynamics. *J Mol Graph*. 1996. doi:10.1016/0263-7855(96)00018-5
24. Kolev VL, Ivanova AN, Madjarova GK, Aserin A, Garti N. Unit cell structure of water-filled monoolein into inverted hexagonal (HII) mesophase modeled by molecular dynamics. J Phys Chem B. 2014. doi:10.1021/jp411138r
25. Briggs J, Chung H, Caffrey M. The temperature-composition phase diagram and mesophase structure characterization of the monoolein/water system. J Phys II. 1996. doi:10.1051/jp2:1996208
26. Borné J, Nylander T, Khan A. Microscopy, SAXD, and NMR studies of phase behavior of the monoolein-diolein-water system. *Langmuir*. 2000. doi:10.1021/la000619e
27. Luzzati V, Vargas R, Mariani P, Gulik A, Delacroix H. Cubic phases of lipid-containing systems: Elements of a theory and biological connotations. *J Mol Biol*. 1993. doi:10.1006/jmbi.1993.1053
28. Salatin S, Maleki Dizaj S, Yari Khosroushahi A. Effect of the surface modification, size, and shape on cellular uptake of nanoparticles. *Cell Biol Int*. 2015. doi:10.1002/cbin.10459
29. Donkor DA, Tang XS. Tube length and cell type-dependent cellular responses to ultra-short single-walled carbon nanotube. *Biomaterials*. 2014. doi:10.1016/j.biomaterials.2013.12.075
30. He C, Hu Y, Yin L, Tang C, Yin C. Effects of particle size and surface charge on cellular uptake and biodistribution of polymeric nanoparticles. *Biomaterials*. 2010. doi:10.1016/j.biomaterials.2010.01.065
31. Zhu M, Nie G, Meng H, Xia T, Nel A, Zhao Y. Physicochemical properties determine nanomaterial cellular uptake, transport, and fate. *Acc Chem Res*. 2013. doi:10.1021/ar300031y
32. Minnelli C, Laudadio E, Mobbili G, Galeazzi R. Conformational insight on WT-and mutated-EGFR receptor activation and inhibition by epigallocatechin-3-gallate: Over a rational basis for the design of selective non-small-cell lung anticancer agents. *Int J Mol Sci*. 2020. doi:10.3390/ijms21051721
33. Ma YC, Li C, Gao F, et al. Epigallocatechin gallate inhibits the growth of human lung cancer by directly targeting the EGFR signaling pathway. *Oncol Rep*. 2014. doi:10.3892/or.2013.2933